Polarization transfer observables in πd elastic scattering

G. Suft and W. Kretschmer
Physikalisches Institut der Universität Erlangen-Nürnberg, D-91058 Erlangen, Germany

E. Boschitz, R. Meier,* and B. Brinkmöller†
Institut für Experimentelle Kernphysik, Universität Karlsruhe, D-76131 Karlsruhe, Germany

B. van den Brandt, P. Hautle, J. A. Konter, and S. Mango
Paul Scherrer Institut, CH-5232 Villigen, Switzerland

L. Mathelitsch
Institut für Theoretische Physik, Universität Graz, A-8010 Graz, Austria

H. Garcilazo
Escuela Superior de Fisica y Matematicas, Instituto Politecnico Nacional, 07738 Mexico City, Mexico

W. Grüebler
Eidgenössische Technische Hochschule Zürich, Eidgenössische Technische Hochschule-Hönggerberg, CH-8093 Zürich, Switzerland

(Received 10 April 2002; published 27 September 2002)

A complete set of πd polarization observables, including polarization transfer, in πd elastic scattering have been measured at backwards scattering angles for two pion energies below and at the $\Delta(3,3)$ resonance. Our results for the analyzing powers are in good agreement with the existing world dataset, while polarization transfer observables have not been measured before. The experimental data are compared to relativistic Faddeev calculations and different Virginia Tech Partial-Wave Analysis Facility solutions, in the laboratory as well as in the center-of-mass system.

DOI: 10.1103/PhysRevC.66.034003 PACS number(s): 24.70.+s, 25.10.+s, 25.80.Dj

I. INTRODUCTION

In medium-energy physics the πNN system has been of great interest in recent years, theoretically as well as experimentally. The reaction channels can be calculated, at least in principle, exactly by relativistic Faddeev calculations making use of the well-known properties of the πN and NN subsystems. Meson-exchange theories may be tested in this few-body system, where pion absorption and emission play an important role. These processes are essential for the understanding of more complex nuclei. The NN-πNN system consists of several strongly interacting channels:

$$\left.\begin{matrix} NN \\ \pi d \end{matrix}\right\} \rightarrow \left\{\begin{matrix} NN \\ \pi d \\ \pi NN \end{matrix}\right.$$

Over the last decades, a number of theoretical models have been developed by various groups, describing the different reaction channels of this system through a set of coupled integral equations [1]. With the continuously increasing database it was possible to test the predictions of these models in more detail. Among the different reaction channels the elastic πd reaction is of special interest: experimentally, because it is a two-body reaction and theoretically, because it can be described by only four complex helicity amplitudes, due to parity and time-reversal invariance. For a model-independent amplitude reconstruction seven independent observables have to be measured. As yet, only five observables have been determined: the differential cross section $d\sigma/d\Omega$, the vector analyzing power iT_{11}, and the tensor analyzing powers T_{20}, T_{21}, and T_{22}, respectively the combined quantities τ_{21}, τ_{22}, and the tensor polarization t_{20} [2–10]. Further independent observables can only be obtained by polarization transfer measurements in a double-scattering experiment.

Some of the already measured observables show systematic discrepancies to the theoretical predictions, mainly at large pion scattering angles $\theta_{\text{c.m.}} > 90°$ and pion energies above the $\Delta(3,3)$ resonance [3,9]. Since different theoretical models [11–15] predict similar results, as long as the same πN and NN subsystems are used, the origin of the deviations between theory and experiment is not to be found in the respective calculations, but either in the underlying two-body input or in a mechanism previously ignored by theoretical approaches. Attempts to understand these discrepancies with contributions of dibaryon resonances failed [16]. Another effort has considered contributions from short-range $N\Delta$ interactions. The parameters were determined by fitting the available experimental data. The phenomenological $N\Delta$ interaction was added in Born terms to the background few-body amplitudes, but only two $N\Delta$-scattering states were found to be important [15]. The experimental data of the differential cross section and the vector analyzing power

*Present address: Physikalisches Institut, Universität Tübingen, D-72076 Tübingen, Germany.

†Present address: SAP AG, D-69185 Walldorf, Germany.

were reproduced very well. However, when terms of higher order were included, it was shown that their influence is not negligible, and they tend to cancel the effects obtained by adding the ΔN interaction only in Born terms [17].

In order to get a consistent theoretical description of all reaction channels in the NN-πNN system, the pion elastic scattering channel has to be coupled to the pion absorption channel via the P_{11} amplitude. Field theoretical considerations [3,14,18] require a separation of the amplitude in a pole and a nonpole part, where the single parts are large but the sum has to be small to reflect the experimental data. However, the predictions of this improved model failed for the tensor polarization t_{20}, respectively the tensor analyzing power T_{20}, in contrast to Faddeev theories where the pole and nonpole parts are small [19]. A possible solution was offered by the Jennings mechanism [20]. Intermediate states containing four particles ($\pi\pi NN$) were considered that strongly suppress the pole part, but further calculations including terms of higher orders showed that the degree of cancellation, especially in the region of the $\Delta(3,3)$ resonance, tended to compensate these effects [21]. The theoretical approach of Jennings and co-workers can be understood as an indication that the treatment of the πNN system may be incomplete, in particular processes containing four particles in the intermediate state have to be considered. This is not included in conventional πNN theories because of the truncation of the Hilbert space to a maximal number of pions. A new theoretical approach by Kvinikhidze and Blankleider should be able to describe these states consistently [22]. It is free from problems of renormalization, based on convolution integrals as well as a consistent four-dimensional relativistic description of the πNN system. This could be a starting point for new theoretical calculations with possible interesting aspects for medium-energy physics.

Since previously the discrepancies between theoretical predictions and experimental data could not be resolved, a model-independent approach would be very useful. To complete the set of experiments needed for a model-independent amplitude reconstruction of the elastic πd channel, at least two polarization transfer observables have to be measured additionally. By polarizing the deuteron target and measuring the polarization of the recoil deuteron, 20 different, but not independent, quantities could be measured. A model-dependent amplitude reconstruction [18] have shown that the measurement of polarization transfer observables with the target spin aligned perpendicular to the scattering plane should have a bigger impact on the helicity amplitudes than a parallel alignment. This and the availability of the polarized target of previous experiments [3] has led to the decision to determine the following four quantities: $(11|11)+(1-1|11)$, $i(11|20)$, $i(11|21)+i(1-1|21)$ and $i(11|22)+i(1-1|22)$. Constraints on the experimental setup due to the target magnetic field enabled measurements at angles between $\theta_{\mathrm{c.m.}}=100°$ and 140° at two incident pion energies, $E_\pi=134$ and 180 MeV, where the differential cross sections and analyzing powers had been measured previously.

Section II gives a brief introduction to the formalism of πd elastic scattering. The experimental setup is described in Sec. III, the data reduction is explained in Sec. IV. A short outline of the relativistic three-body equations as a basis of a model calculation is given in Sec. V. Finally the experimental results are represented in Sec. VI and compared with the predictions of the Faddeev calculations and two solutions of the Virginia Tech Partial-Wave Analysis Facility (SAID) analyses.

II. FORMALISM

In the helicity formalism introduced by Jacob and Wick [23], elastic πd scattering is defined by four complex helicity amplitudes due to parity and time-reversal invariance. The relations between observables and the helicity amplitudes have been stated previously [24,25]. In order to give the connection to the experimental quantities, for easier reference and to clarify conventions and notations, we repeat some definitions and equations (see Sec. 1 in the Appendix). The reaction parameters are labeled (target|recoil) $=(LM|L'M')$. There are 16 linearly independent observables [24,25]: the differential cross section $d\sigma/d\Omega$, one vector, three tensor polarizations t_{LM}, and 20 polarization transfer coefficients (nine of them are linearly dependent). The following polarization observables were accessible in our experiment, at least as linear combinations:

$$it_{11}=-i(00|11),\quad t_{20}=(00|20),$$

$$t_{21}=-(00|21),\quad t_{22}=(00|22),$$

$$(11|11)+(1-1|11),\quad i(11|20),$$

$$i(11|21)+i(1-1|21),\quad i(11|22)+i(1-1|22),$$

where it_{11}, t_{20}, t_{21}, and t_{22} are the vector and tensor polarizations following the Madison convention. The transformation of the reaction parameters from the center-of-mass system in the laboratory system can be calculated from the expression [24]

$$(LM|L'M')_{\mathrm{lab}}=\sum_{M''}(LM|L'M'')d^{L'}_{M''M'}(-\theta_R), \qquad (1)$$

where θ_R is the deuteron recoil angle in the laboratory system and $d^{L'}_{M''M'}$ are Wigner rotation matrices. This formula applies also for the transformation from the laboratory to the center-of-mass system, with an additional sign change of the recoil angle.

To obtain the reaction parameters in the Madison convention, an additional sign factor has to be taken into account:

$$(LM|L'M')^{Mad}=(-1)^{L+M+M'}(LM|L'M'). \qquad (2)$$

For a complete determination of the four complex helicity amplitudes, except a common phase factor, at least seven independent observables have to be measured. So far, only five of them have been determined at several energies in the region of the $\Delta(3,3)$ resonance, namely the differential cross section and four polarization observables. In principle, there are two different experimental setups: a single-scattering experiment with a polarized deuteron target and a double-scattering experiment, where the polarization states of the

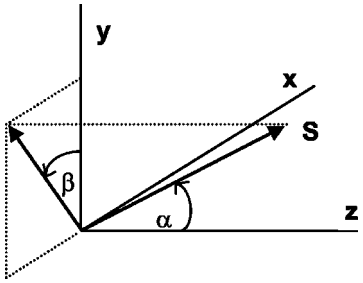

FIG. 1. The quantization axis S of the deuteron spins relating to a coordinate system defined by the Madison convention. α is the polar angle measured from the z axis, and β is measured from the y axis to the projection of S in the xy plane.

outgoing deuterons have to be analyzed. In order to obtain further independent observables of the πd system, polarization transfer observables have to be measured, where both methods have to be combined ($\vec{d}(\pi,\pi)\vec{d}$), which means the measurement of the polarization states of the initial and final channel. The rescattered deuterons may have the following seven polarization components:

$$it_{11},\ it_{1-1},\ t_{20},\ t_{21},\ t_{2-1},\ t_{22},\ \text{and}\ t_{2-2}.$$

Several different polarization transfer coefficients could be determined, depending on the alignment of the target polarization relative to the scattering plane.

A. The target polarization

The direction of the target magnetic field fixes the orientation of the deuteron spins in the target material. Their quantization axis S may be parallel or antiparallel to the magnetic field. Generally it does not correspond with the z axis of a coordinate system according to the Madison convention [26] (see Fig. 1). The target magnetic field was aligned perpendicularly to the scattering plane. This choice has physical [18] as well as technical advantages, all particles being in one plane. In this special case are $\alpha=90°$ and $\beta=0°$ (spin ''up'') and $\beta=180°$ (spin ''down''), respectively. Therefore t_{10} and $t_{2\pm1}$ are zero.

$$t_{11}=t_{1-1}=\mp i\sqrt{\frac{3}{2}}p_Z,$$

$$t_{20}=-\frac{1}{2\sqrt{2}}p_{ZZ},\quad t_{22}=t_{2-2}=-\sqrt{\frac{3}{4}}p_{ZZ}. \tag{3}$$

B. The polarization of the recoil deuterons

The polarization state of the recoil deuteron has been determined by the reaction $^3\mathrm{He}(\vec{d},p)^4\mathrm{He}$. Due to parity invariance this cross section can be written as

$$\sigma(\theta)=\sigma_0(\theta)[1+2it_{11}iT_{11}(\theta)+t_{20}T_{20}(\theta)+2t_{21}T_{21}(\theta)+2t_{22}T_{22}(\theta)]. \tag{4}$$

$\sigma_0(\theta)$ is the cross section for unpolarized deuterons, t_{kq} are the polarization components of the incident deuterons, and $T_{kq}(\theta)$ are the analyzing powers of the reaction $^3\mathrm{He}(d,p)^4\mathrm{He}$. The azimuthal dependence of the emitted protons is expressed in the outgoing reactant helicity frame which is obtained by a rotation of the projectile helicity frame [27]:

$$\sigma(\theta,\phi)=\sigma_0(\theta,\phi)[1+2it_{11}iT_{11}(\theta)\cos\phi+t_{20}T_{20}(\theta)+2t_{21}T_{21}(\theta)\cos\phi+2t_{22}T_{22}(\theta)\cos2\phi]. \tag{5}$$

Nine counter telescopes were mounted at three different scattering angles $\theta=0°,25°,45°$ and four azimuthal angles $\phi=0°$ (left), 90° (down), 180° (right), 270° (up). The counting rates are labeled $L(\theta_i),D(\theta_i),R(\theta_i)$, and $U(\theta_i)$, respectively ($\theta_i\in\{25°,45°\}$), and $N(0°)$ for the 0° detector.

There are two different methods to determine the polarization states of the recoil deuterons:

(a) The ratio method uses proton counting rates at different polar and azimuthal angles.

(b) The absolute method needs the measurement of the incident recoil deuterons N_d. To identify these deuterons a more complicated experimental setup is needed.

The ratio and absolute methods are independent of each other and therefore allow two independent determinations of the polarization states (see Sec. 2 in the Appendix). The polarimeter has to be calibrated with unpolarized and polarized deuteron beams to obtain its efficiencies and analyzing powers [28]. The formulas for the absolute and the ratio method can be found in Ref. [28] and in the Appendix.

C. The polarization transfer parameters

The polarization transfer parameters $(kq|k'q')^{\mathrm{Mad}}$ in the Madison convention can be calculated from the target and recoil polarizations t_{kq} and $t_{k'q'}$, respectively. The indices $0,\pm$ indicate the target magnetic field direction, either unpolarized or aligned parallel and antiparallel to the scattering plane:

$$t^{\pm}_{k'q'}\sigma^{\pm}=\sigma_0\left[t^0_{k'q'}+\sum_{k,q}t^{\pm}_{kq}(kq|k'q')\right]. \tag{6}$$

Inserting Eqs. (3) yields

$$t^{\pm}_{k'q'}\sigma^{\pm}=\sigma_0\left\{t^0_{k'q'}\mp\sqrt{\frac{3}{2}}p_Zi[(11|k'q')+(1-1|k'q')]-\frac{p_{ZZ}}{2\sqrt{2}}\left[(20|k'q')+\sqrt{6}[(22|k'q')+(2-2|k'q')]\right]\right\}. \tag{7}$$

Specific choices of the final states $k'q'$ and either subtraction or addition of the two possibilities (spin parallel and antiparallel) and using Eq. (2) gives:

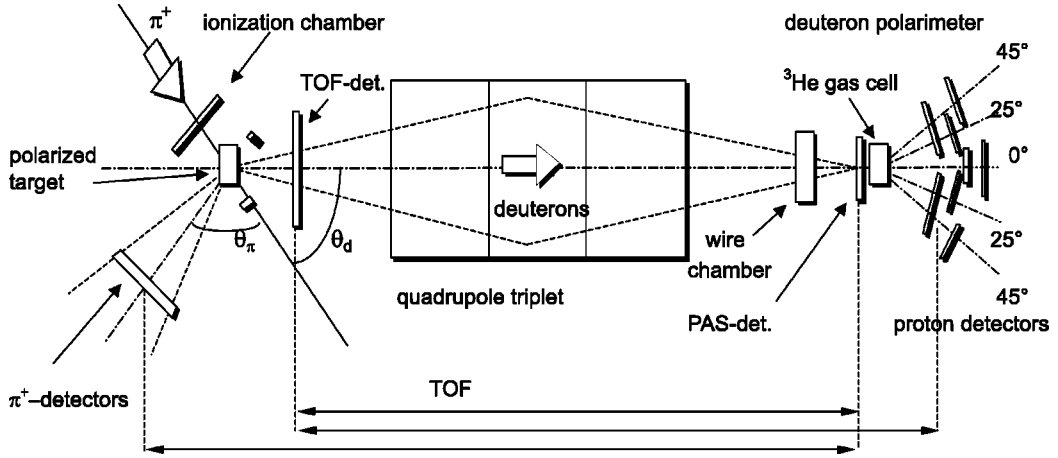

FIG. 2. Schematic diagram of the experimental setup of the double-scattering apparatus.

$$
\begin{aligned}
&(1\pm1|11)^{\mathrm{Mad}} \\
&\quad=-\frac{1}{\sqrt{3}p_Z}\left[\frac{(it_{11}^{+}+it_{1-1}^{+})\sigma^{+}-(it_{11}^{-}+it_{1-1}^{-})\sigma^{-}}{2\sigma^{0}}\right], \\
&i(11|20)^{\mathrm{Mad}}=-\frac{1}{\sqrt{3}p_Z}\left[\frac{t_{20}^{+}\sigma^{+}-t_{20}^{-}\sigma^{-}}{2\sigma^{0}}\right], \\
&i(1\pm1|21)^{\mathrm{Mad}}=\frac{1}{\sqrt{3}p_Z}\left[\frac{(t_{21}^{+}-t_{2-1}^{+})\sigma^{+}-(t_{21}^{-}-t_{2-1}^{-})\sigma^{-}}{2\sigma^{0}}\right], \\
&i(1\pm1|22)^{\mathrm{Mad}}=-\frac{1}{\sqrt{3}p_Z}\left[\frac{(t_{22}^{+}+t_{2-2}^{+})\sigma^{+}-(t_{22}^{-}+t_{2-2}^{-})\sigma^{-}}{2\sigma^{0}}\right],
\end{aligned}
\tag{8}
$$

with

$$
(L\pm M|L'M')^{\mathrm{Mad}}=(LM|L'M')^{\mathrm{Mad}}+(L-M|L'M')^{\mathrm{Mad}}.
$$

The connection to the observables in the cartesian frame is given in the Appendix.

III. EXPERIMENTAL SETUP

In order to determine polarization transfer observables, the polarization states in the initial and the final channel have to be measured. This requires a polarized deuteron target and a polarimeter to analyze the recoil deuterons in a double-scattering experiment.

The measurements were performed at the $\pi E1$ channel of the Paul Scherrer Institut (PSI) with the double-scattering apparatus shown schematically in Fig. 2.

Since the pion rate was too high (approximately 5×10^{8} π^{+}/s) to allow individual counting of pions, an ionization chamber was used to get absolute normalization. Careful monitoring of the pion beam was required, especially since the target was smaller than the beam spot, and small shifts would have changed the luminosity of the reaction and therefore the reaction rate. This was achieved by an additional luminosity monitor. The reaction $d(\pi,p)p$ is insensitive to the target polarization at a scattering angle of $\theta_{\mathrm{c.m.}}=90°$. Three scintillation counters were used for a coincidence measurement of the outgoing protons, one ΔE-ΔE telescope at the left side (ΔE_L and E_L) and a ΔE counter at the right side (E_R). The pions were detected in coincidence with the recoil deuterons using three 2 mm thick plastic scintillators with a total area of 400×300 mm^2. Photomultipliers were mounted on both ends of the scintillator panels and allowed a crude position resolution. A quadrupole triplet was placed between target and polarimeter to increase the acceptance solid angle and to reduce background, mainly from protons.

A. The polarized deuteron target

The target system consisted of two main components: a superconducting Helmholtz coil supplying a field strength of $B=2.5$ T with a homogeneity of $\Delta B/B=3\times10^{-4}$ over the target volume and a ^{3}He/^{4}He dilution refrigerator with a cooling power of approximately 1 mW at 100 mK integrated in a single cryostat (see Fig. 3). The ^{4}He bath of the cryostat was used for both cooling of the superconducting coils and condensing the ^{3}He/^{4}He mixture. Dynamic polarization of the target material was produced by irradiating the target with microwaves of approximately 69.9 GHz (for positive polarization) and 70.2 GHz (for negative polarization). Inversion of the polarization did not involve therefore reversing the polarity of the magnetic field. The target material consisted of deuterated ammonia ND_3, in the form of approximately 1 mm diameter chunks contained in a cylindrical cell with 18 mm diameter and 18 mm height. The paramagnetic radicals were created by irradiating the material under liquid argon at 90 K with electrons from the 20 MeV injection linac of the Bonn synchrotron. Compared with deuterated alcohols (for example propandiol), ND_3 and LiD have a higher radiation resistance and a higher spin density. A test run, however, showed that the background from quasifree deuteron scattering on ^{6}Li is much too high to separate it exactly from the elastic πd scattering; therefore ND_3 was chosen as target material.

B. The deuteron polarimeter

The deuteron polarimeter was built by Grüebler *et al.* [28] and is divided in two main components: the scintillation

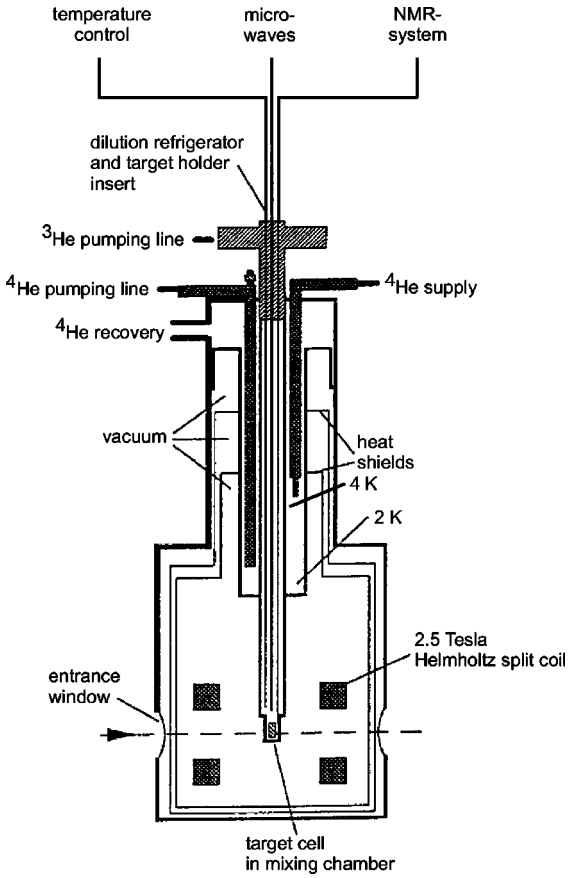

FIG. 3. Schematic view of the polarized deuteron target.

counters to detect the protons from the ^{3}He(d,p) reaction and a vacuum chamber containing a position-sensitive wire chamber, a scintillator and the ^{3}He-target cell (see Fig. 4). The ^{3}He$(\vec{d},p)^4$He reaction has many advantages, in particular the high Q value of 18.4 MeV enabling a clear separation of the protons from background. The position of the incident deuterons was determined by a wire chamber. This was necessary because the effective solid angle of the outgoing proton detectors varies when the deuteron beam deviates from the symmetry axis of the polarimeter. Possible systematic errors stemming from such an asymmetry were therefore eliminated.

The wire chamber was mounted in a pressure vessel inside the vacuum chamber in front of the second time-of-flight detector (PAS detector) and the ^{3}He cell. The position-sensitive zone was 38×38 mm^2 and therefore bigger than the entrance window of the target cell. The counting wires were made of 20 μm thick tungsten wires, with a 2 mm vertical and horizontal grid resolution. Entrance and exit windows consisted of a 100 μm thin Mylar foil in order to minimize the energy loss of the deuterons. The operational mixing was 89.1% argon, 10% isobutan, and 0.9% freon. A voltage of -4.4 kV was applied and the counting efficiency was 80%. The signals were collected by delay-line read-out. For the detection of the recoil deuterons the time of flight (TOF) through the quadrupole triplet was measured by two detectors (TOF, PAS) (see Fig. 2). They were also used for several other time-of-flight measurements.

The TOF detector was located in front of the vacuum entrance window of the triplet and had a sensitive area of

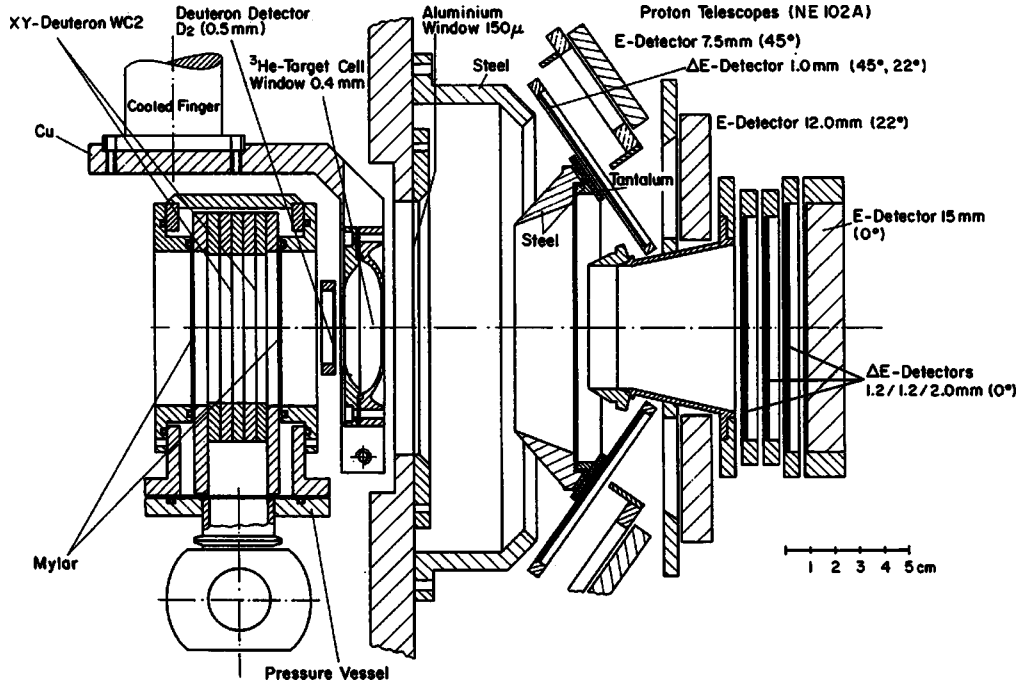

FIG. 4. Side view of the deuteron polarimeter [28].

200 mm^2 and was 0.5 mm thick. The signals were read out through a 500 mm long light guide, in order to protect the photomultiplier from influences of the target magnetic field.

The PAS detector was adjusted between the wire chamber and the entrance window of the ^{3}He cell, with a sensitive area of 32 mm diameter. The effective length of the ^{3}He cell was 15 mm and its entrance window had a diameter of 32 mm and was 0.2 mm thick. The exit window had a shape such that the protons of various angles reach the detectors with the same energy; the thickness was 0.4 mm. Both were made from a special aluminum alloy, Peruval-215.

In order to maximize the efficiency of the polarimeter, the target was cooled down to 14 K, and the pressure of the ^{3}He gas was 12 bar. The target temperature was monitored with three diodes and was read out together with the pressure in fixed time intervals. Several layers of thin aluminized Mylar foil guaranteed a thermal isolation of the cell. The vacuum chamber was evacuated to 10^{-7} mbar to avoid condensation of residual gas on the target surface. For the determination of the polarization components it_{11}, t_{20}, t_{21}, and t_{22} several proton detectors were mounted at different scattering (θ) and azimuthal (ϕ) angles:

(1) at $\theta=0°$ one counter telescope with four scintillation detectors [P00 (1.2 mm), P09 (1.2 mm), P9 (2 mm), and P10 (15 mm), consecutively in beam direction];

(2) at $\theta=25°$ four scintillation counters, 12 mm thick, at four different azimuthal angles [P1 ($\phi=0°$), P2 ($\phi=180°$), P3 ($\phi=90°$), and P4 ($\phi=270°$)];

(3) at $\theta=45°$ four scintillation counters, 7.5 mm thick, at four different azimuthal angles [P5 ($\phi=0°$), P6 ($\phi=180°$), P7 ($\phi=90°$), and P8 ($\phi=270°$)].

The ΔE counters [$P0L$ (left), $P0D$ (down), $P0R$ (right), and $P0U$ (up)] were 1 mm thick, each for two E counters at $\theta=25°$ and 45° and for one azimuthal angle. To ensure a fast adjustment of the polarimeter, the whole frame was mounted on a transversal sliding system, which was additionally rotatable around the polarimeter axis.

Several components were changed compared to the original design [28]: The ΔE counter P00 was mounted at $\theta=0°$. Energy loss and straggling of the incoming deuterons were reduced by a thinner entrance window of the ^{3}He cell (0.2 mm). This enabled also measurements at smaller pion scattering angles. The resulting difference in the deuteron energy to the calibration data [28] was considered by energy loss calculations and was included in the analysis. The aluminum absorbers and the solid state detector were removed.

C. The data acquisition

In this double-scattering experiment a background suppression of 1 to 10^{-6} had to be reached. This was necessary because of the large amount of background protons and the polarimeter efficiency of 10^{-4}.

Three different independent trigger systems were used and each was read out from its own front end computer:

(i) The pp data acquisition for the luminosity monitor [$d(\pi,p)p$ reaction]: The high rate of random coincidences, resulting from other (π,p) reactions and a possible contamination of the pion beam, were suppressed in the off-line analysis. A proton event was defined by a coincidence $\Delta E_L \times E_L \times E_R$. The corresponding timing window was 100 ns wide, ensuring an off-line selection of protons coming from the deuteron breakup reaction. The time-of-flight signal between the detectors on the left and right side and an additional random coincidence left/right coming from different, successive beam bursts made an online monitoring of the πd luminosity possible.

(ii) The πd data acquisition to measure σ_0 and $\sigma^{\pm}$, respectively: A pion was defined by a coincidence π_L(up) $\times \pi_R$(up) or π_L(mid) $\times \pi_R$(mid) or π_L(down) $\times \pi_R$(down), a deuteron by a coincidence TOF$\times$PAS. For events ''pion-deuteron'' an additional ''π bit,'' defined by the kinematical coincidence between pion and deuteron, was recorded. To ensure a proper selection of πd events time-of-flight signals between pion detector/TOF, pion detector/PAS, and TOF/PAS were used.

(iii) The polarimeter data acquisition: The trigger logic was built up in analogy to the πd data acquisition, but additionally a polarimeter event was demanded. A proton detected in the polarimeter was defined by the following coincidence: $P00 \times P09 \times P9 \times P10$ ($\theta=0°$) or $P0L \times P1$ or $P0L \times P5$ ($\theta=25°$ and 45°,$\phi=0°$) or $P0R \times P2$ or $P0R \times P6$ ($\theta=25°$ and 45°,$\phi=180°$) or $P0D \times P3$ or $P0D \times P7$ ($\theta=25°$ and 45°,$\phi=90°$) or $P0U \times P4$ or $P0U \times P8$ ($\theta=25°$ and 45°,$\phi=270°$).

IV. THE DATA RECONSTRUCTION

The data analysis included a series of one- and two-dimensional software cuts. Although the thresholds and the high voltage of the photomultipliers were checked continuously during the experiment, the raw spectra were inspected before the analysis to guarantee stable and constant conditions. The luminosity of the πd reaction was monitored via the rates of the $d(\pi,p)p$ reaction and the ionization chamber. In the first data-taking period a relative value of the target polarization was determined online by NMR and its absolute value was calculated, measuring the polarized differential cross section of the elastic πd scattering. During the second data-taking period it was possible to obtain an absolute value of the deuteron polarization by measuring the NMR signal at thermal equilibrium. The polarization states of the rescattered deuterons were extracted from the spectra of the proton detectors in the polarimeter and the time-of-flight spectra of the corresponding deuterons.

A. The beam monitor

The pion flux incidenting on the deuteron target was monitored by detecting the two protons from the $d(\pi,p)p$ reaction in kinematic coincidence at $\theta_{\text{c.m.}}=90°$. To get rid of the main part of the random events several software cuts on the time-of-flight and energy spectra of the three proton detectors were performed. Figure 5 shows a three-dimensional histogram of the energy losses in the detectors $\Delta E_L \times E_R$ before and after this background subtraction. The 20 ns time structure and the rate of the pion beam were responsible for the large number of background events. Constructing poly-

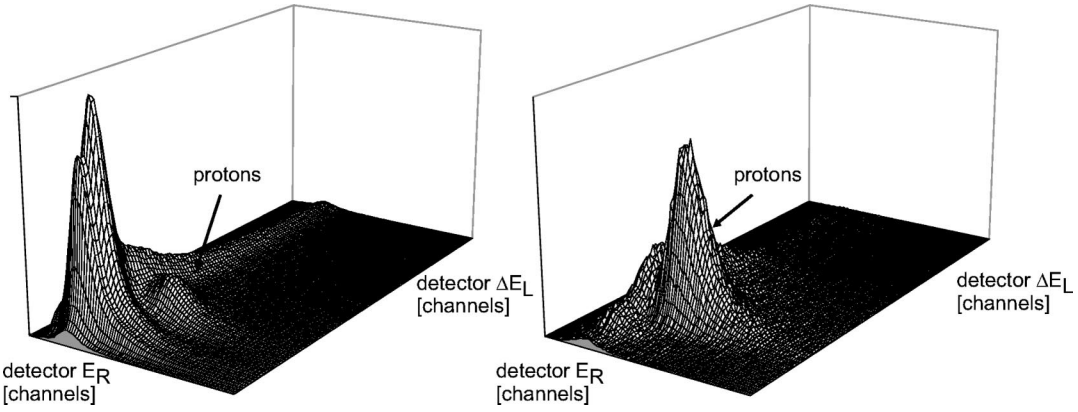

FIG. 5. Three dimensional energy loss spectra of the luminosity monitor ($\Delta E_L \times E_R$) without (left) and with (right) background reduction.

gons on the two-dimensional projections of this histogram and the corresponding proton spectra $\Delta E_L \times E_L$ and $E_L \times E_R$, defining the protons, enabled an effective background reduction. The obtained breakup events were normalized to the primary beam intensity on the ionization chamber. Runs with slightly varying luminosity were not used for the determination of the deuteron target polarization.

B. The target polarization

The target polarization was monitored by measuring the NMR absorption signal every 5 min. There was a slight decrease of the target polarization during each data run, possibly due to beam heating effects. The absolute value of the polarization can be deduced directly from

$$p_Z(\mathrm{dyn}) = \frac{A(\mathrm{dyn})}{A(\mathrm{TE})} p_Z(\mathrm{TE}),$$

where $p_Z(\mathrm{TE})$ is the value of the target polarization at thermal equilibrium, given by the Boltzmann distribution, $A(\mathrm{TE})$ and $A(\mathrm{dyn})$ are the areas under the NMR signal at thermal equilibrium and dynamically polarized, respectively. Since it is very difficult to measure the NMR signal of deuterated ammonia (ND_3) at thermal equilibrium, the deuteron polarization was determined independently by measuring the relative πd elastic cross section. The dynamic polarization $p_Z(\mathrm{dyn})$ was determined in the second data-taking period from the ratio of the areas $A(\mathrm{dyn})/A(\mathrm{TE})$ and $p_Z(\mathrm{TE})$. Both measurements agree very well. The target polarization determined via the NMR measurement was $p_Z(\mathrm{dyn}) = A(\mathrm{dyn}) \times (4.060 \pm 0.193) \times 10^{-6}$, the measurement of the relative differential cross section resulted in $p_Z(\mathrm{dyn}) = A(\mathrm{dyn}) \times (3.912 \pm 0.162) \times 10^{-6}$.

To use the method mentioned above the differential cross section for πd elastic scattering with polarized and unpolarized deuteron target had to be measured, no absolute normalization was required. The pions and deuterons were detected in kinematical coincidence. Their counting rate was determined from the energy loss and time-of-flight signals of one of the pion detectors and the TOF and PAS detectors. The main contribution of background events arose from random coincidences, due to the time structure of the beam, and from other reaction mechanisms, for example elastic scattering on He and ^{3}He breakup. The final analysis was performed in two steps. Cuts on the prompt peaks in the time-of-flight spectra enabled the separation of events which had the ''right timing.'' Finally, polygons were constructed around the πd elastic events identified in two-dimensional spectra of the deuteron time-of-flight versus energy loss in the TOF and PAS detectors. By normalizing the number of these events to the incoming beam intensity, one obtains the relative πd cross section ($\sigma^{\pm}$ is the differential cross section for positive and negative polarization p_Z, σ^0 for zero polarization):

$$\sigma^{\pm} = \sigma^0 \left(1 \pm \sqrt{3} i T_{11} p_Z^{\pm} - \sqrt{\frac{3}{2}} \tau_{22} p_{ZZ}^{\pm} \right).$$

The angular distribution of the analyzing power iT_{11} has been measured in former experiments over the full angular range with small errors [3,4,6]. These values were taken to determine the target polarization:

$$p_Z = \frac{1}{\sqrt{3} i T_{11}} \frac{\sigma^+ - \sigma^-}{2\sigma^0},$$

$$p_{ZZ} = 2 - \sqrt{4 - 3 p_Z^2}.$$

The results of the polarization measurement at different pion energies T_π and center-of-mass scattering angles $\theta_{\mathrm{c.m.}}$ are listed in Table I. $\overline{p_Z}$ and $\overline{p_{ZZ}}$ are the averaged values of the vector and tensor polarization, respectively. Δp_Z and Δp_{ZZ} include both statistical and systematic errors. The main contribution results from the experimental uncertainty $\Delta i T_{11}$ coming from literature.

C. The deuteron polarization

The polarization states of the recoil deuteron beam were determined using the $^3\mathrm{He}(\vec{d},p)^4\mathrm{He}$ reaction and detecting the outgoing protons at $\theta = 0°, 25°, 45°$ and $\phi = 0°, 90°, 180°, 270°$. The selection of $^3\mathrm{He}(d,p)^4\mathrm{He}$ events in the presence of a large background was a critical factor in the analysis. For incident deuteron energies 16 MeV $\leqslant E_d \leqslant$ 30 MeV

TABLE I. Vector (p_Z) and tensor polarization (p_{ZZ}) of the ND_3 target during the experiment.

	$T_\pi = 134$ MeV $\theta_{\pi,\text{c.m.}} = 136°$	$T_\pi = 180$ MeV $\theta_{\pi,\text{c.m.}} = 108°$	$T_\pi = 180$ MeV $\theta_{\pi,\text{c.m.}} = 108°$	$T_\pi = 180$ MeV $\theta_{\pi,\text{c.m.}} = 127°$
p_Z^+	0.264 ± 0.010	0.267 ± 0.010	0.225 ± 0.011	0.277 ± 0.010
p_Z^-	0.237 ± 0.010	0.219 ± 0.010	0.195 ± 0.009	0.241 ± 0.010
$\overline{p_Z}$	0.251 ± 0.010	0.243 ± 0.010	0.215 ± 0.007	0.259 ± 0.010
$\overline{p_{ZZ}}$	0.0478 ± 0.0039	0.0448 ± 0.0037	0.0350 ± 0.0023	0.0510 ± 0.0040

the corresponding protons were stopped in the E detectors of the ΔE-E telescopes. These events were separated from background protons and deuterons with higher energy by constructing polygons on the two-dimensional pulse height spectra ΔE versus E. Software filters assured an associated incoming deuteron from elastic πd scattering. The determination of these deuterons was done similarly to the πd cross section (previous subsection). Nevertheless, the deuteron rate appearing in the time-of-flight spectra was strongly suppressed because of the polarimeter efficiency of 10^{-4} and the trigger condition that particles had to reach one of the E detectors of the polarimeter. Deuterons and protons that had enough kinetic energy to be detected in the polarimeter are separated by their time of flight (see Fig. 6). Accidental coincidences induced by protons of the following beam burst were excluded by the electronics setup and by building difference spectra of the TDCs.

The used combination of software and hardware filters ensured a clear separation of protons from the $^3\text{He}(d,p)$ reaction and the large number of background events. This technique was additionally checked by background target runs, replacing ND_3 with NH_3 and in the polarimeter ^{3}He with ^{4}He. A typical spectrum (foreground) of the time of flight versus energy loss in the E detectors is shown in Fig. 7 left, the background spectrum with ^{4}He in the polarimeter target cell in Fig. 7 right. The deuteron beam profiles from the wire chamber were checked for unfiltered and filtered events. Together with the polarimeter efficiencies $r(\theta_i)$ and analyzing powers iT_{11}, T_{20}, T_{21}, and T_{22} the polarization of the recoil deuteron beam could be determined with the ratio and the absolute method.

V. THEORY

The following theoretical predictions were obtained with the formalism developed in Ref. [29] in which the relativistic Faddeev equations are solved applying the spectator-on-mass-shell approximation. In this formalism one uses as input the nucleon-nucleon $^1S_0$, $^3S_1$, and $^3D_1$ channels and the pion-nucleon S_{11}, S_{31}, P_{11}, P_{13}, P_{31}, and P_{33} channels in a full three-body calculation. In addition, all pion-nucleon D, F, and G waves are taken into account in the $\pi d \to \pi d$ single-scattering term.

A. Relativistic three-body equations

We start with the Bethe-Salpeter equation for three particles such that it sums all diagrams in which two particles interact in all possible ways while the third particle acts as spectator (that is we neglect three-body forces). This equation, for the case when particles 2 and 3 are initially forming a bound state and particle 1 is free, can be written in Faddeev form as

$$T_i = (1-\delta_{i1})t_i + \frac{1}{(2\pi)^4}\sum_{j\neq i}\int d^4k_j' t_i G_j G_k T_j, \qquad (9)$$

where T_i is the sum of all the diagrams in which particles j and k interact while particle i acts as spectator. t_i is the scattering amplitude of the pair jk, that is, the sum of all the possible diagrams where particles j and k are in the initial and final state with particle i as spectator. We show this equations in diagrammatic form in Fig. 8.

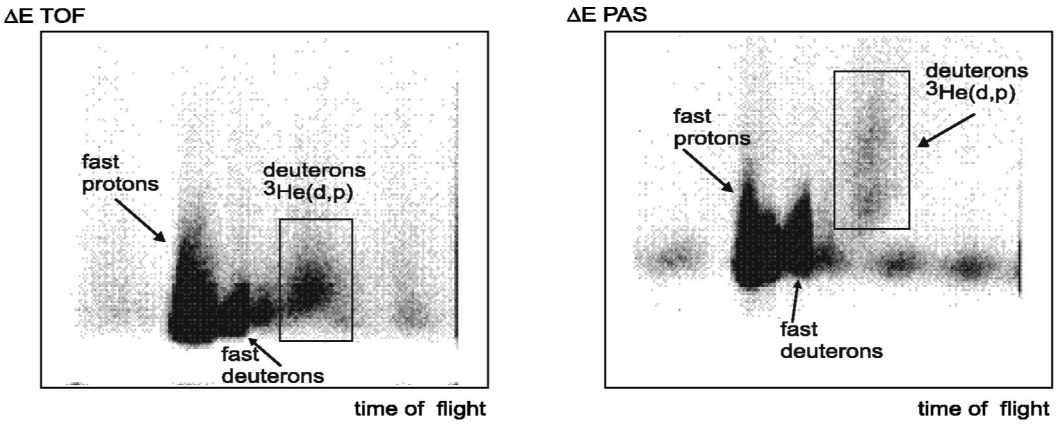

FIG. 6. Two-dimensional spectrum of time-of-flight difference between TOF and PAS detector (horizontal axis) and pulse height in the TOF (left) and PAS detector (right) (vertical axis), for $T_\pi = 180$ MeV and $\theta_{\text{c.m.}} = 108°$.

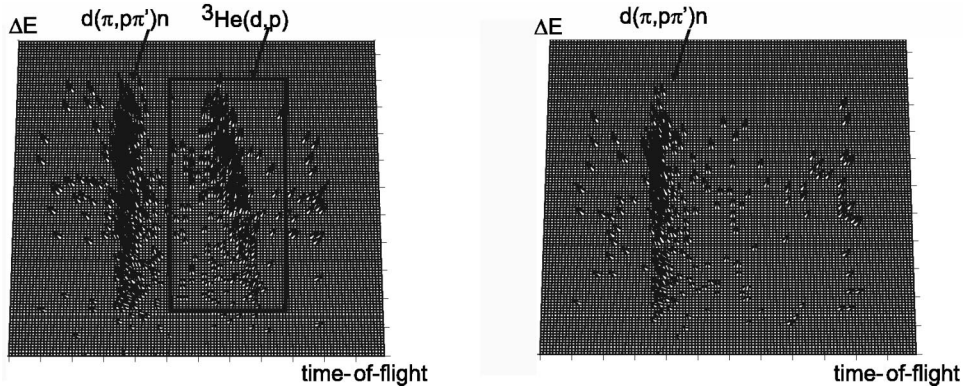

FIG. 7. Two-dimensional spectrum of time-of-flight between TOF and PAS detector versus pulse height of E counters in the polarimeter at $\theta=45°$, containing all filters, left: with ^{3}He and right: with ^{4}He in the polarimeter target cell, for $T_\pi=180$ MeV and $\theta_{\text{c.m.}}=108°$.

In order to obtain three-dimensional integral equations, we integrate over the fourth component of k_j' by closing the contour from below in the complex k_{j0}' plane and by assuming that only the pole in G_j at $k_{j0}'=\sqrt{\vec{k}_j\,'^2+m_j^2}-i\epsilon\equiv\omega_j'-i\epsilon$ contributes to the integral [19]. Thus, Eq. (9) becomes a three-dimensional integral equation

$$T_i=(1-\delta_{i1})t_i-\frac{i}{(2\pi)^3}\sum_{j\neq i}\sum_{\nu_j'}\int\frac{1}{2\omega_j'}d\vec{k}_j'\,t_i|\vec{k}_j'\,\nu_j'\rangle \times\langle\vec{k}_j'\,\nu_j'|G_kT_j, \tag{10}$$

where $|\vec{k}_j'\,\nu_j'\rangle$ is a single-particle plain-wave state of momentum $\vec{k}_j'$ and helicity ν_j'.

B. Partial-wave decomposition

We will consider the integral equations of the previous subsection in the three-body center-of-mass frame defined by

$$\vec{k}_i+\vec{k}_j+\vec{k}_k=\vec{0}. \tag{11}$$

The three particles have spins and isospins s_i, s_j, s_k and τ_i, τ_j, τ_k, such that $\vec{k}_i$, $\vec{k}_j$, $\vec{k}_k$ and ν_i, ν_j, ν_k are the momenta and helicities of the three particles measured in the three-body center-of-mass frame defined by Eq. (11). Then, as shown in Ref. [29], the partial-wave basis states are of the form

$$|q_ip_i;\alpha_i\rangle\equiv|q_ip_i;\nu_iJMl_iS_ij_im_iI_i\tau_iIM_I\rangle, \tag{12}$$

where q_i is the magnitude of the relative three-momentum between particle i and the center of mass of the pair jk measured in the three-body center-of-mass frame and p_i is the magnitude of the relative three-momentum between particles j and k measured in the two-body center-of-mass frame. ν_i, J, and M are the helicity of particle i, the total angular momentum of the system, and its third component, respectively. l_i and S_i are the orbital angular momentum and spin of the pair jk while j_i and m_i are the total angular momentum and helicity of the pair jk. Finally, I_i, τ_i, I, and M_I are the isospin of the pair jk, the isospin of particle i, the total isospin of the system, and its third component, respectively.

As it has been shown in Ref. [29], with the basis states (12) the three-body integral equation takes the partial-wave form

$$\langle q_ip_i;\alpha_i|T_i|\phi_0\rangle=(1-\delta_{i1})\langle q_ip_i;\alpha_i|t_i|\phi_0\rangle-\frac{i}{(2\pi)^3}\sum_{j\neq i}\sum_{\alpha_i'}\sum_{\alpha_j}\times\int\frac{\omega(p_i')}{W_i(p_i'q_i')}\frac{p_i'^2dp_i'q_i'^2dq_i'}{2\omega_i(q_i')2\omega_j(p_i')2\omega_k(p_i')}\frac{\omega(p_j)}{W_j(p_jq_j)} \times\frac{p_j^2dp_jq_j^2dq_j}{2\omega_j(q_j)2\omega_k(p_j)2\omega_i(p_j)}\langle q_ip_i;\alpha_i|t_i|q_i'p_i';\alpha_i'\rangle\times\langle q_i'p_i';\alpha_i'|q_jp_j;\alpha_j\rangle G_0(k_k')\langle q_jp_j;\alpha_j|T_j|\phi_0\rangle, \tag{13}$$

where

$$\omega_i(k)=(m_i^2+k^2)^{1/2}, \tag{14}$$

$$\omega(p_i)=\omega_j(p_i)+\omega_k(p_i), \tag{15}$$

$$W_i(q_ip_i)=[\omega^2(p_i)+q_i^2]^{1/2}. \tag{16}$$

For the deuteron wave function that appears in the initial state $|\phi_0\rangle$ and in the final state $\langle\phi_0|$ we used the Paris model [31] as described in Ref. [29] while the recoupling coefficients $\langle q_i'p_i';\alpha_i'|q_jp_j;\alpha_j\rangle$ were described in detail in Refs. [29,30].

C. Two-body amplitudes

The pion-nucleon scattering amplitude t_i taken between partial-wave states (12) has the form

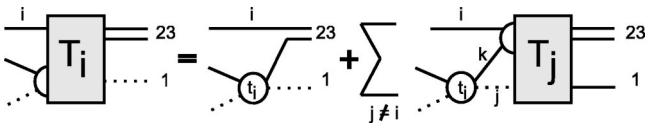

FIG. 8. Diagrammatic form of Eq. (9).

$$\langle q_i p_i;\alpha_i|t_i|q_i' p_i';\alpha_i'\rangle = \delta_{\nu_i\nu_i'}\delta_{JJ'}\delta_{MM'}\delta_{l_i l_i'}\delta_{S_i S_i'}\delta_{j_i j_i'}\delta_{m_i m_i'}\delta_{I_i I_i'}\delta_{II'}\delta_{M_I M_I'} \times 2\omega_i(q_i)\frac{1}{q_i^2}\delta(q_i-q_i')\langle p_i|t_i^{l_i j_i I_i}(s_i)|p_i'\rangle, \tag{17}$$

where

$$s_i = S + M^2 - 2\sqrt{S(M^2+q_i^2)} \tag{18}$$

is the invariant mass squared of the two-body subsystem and S is the invariant mass squared of the three-body system.

We have parametrized the off-shell partial-wave pion-nucleon t matrices that appear in Eq. (17) as

$$\langle p_i|t_i^{l_i j_i I_i}(s_i)|p_i'\rangle = \left(\frac{p_i}{p_0}\right)^{l_i} g(p_i,p_0)\langle p_0|t_i^{l_i j_i I_i}(s_i)|p_0\rangle \times\left(\frac{p_i'}{p_0}\right)^{l_i} g(p_i',p_0), \tag{19}$$

where p_0 is the on-shell momentum given by

$$p_0^2 = \frac{[s_i-(M+\mu)^2][s_i-(M-\mu)^2]}{4s_i}, \tag{20}$$

and the form factor $g(p_i,p_0)$ was taken to be

$$g(p_i,p_0) = \frac{\Lambda^2+p_0^2}{\Lambda^2+p_i^2}, \tag{21}$$

with the cutoff parameter

$$\Lambda = 600 \ \text{MeV}/c. \tag{22}$$

For the on-shell partial-wave pion-nucleon t matrices $\langle p_0|t_i^{l_i j_i I_i}(s_i)|p_0\rangle$ in the physical region $s_i>(M+\mu)^2$ we used the values of the Virginia Polytechnic Institute Group [32], obtained through the SAID dial-in system. In the unphysical region $0<s_i<(M+\mu)^2$ we used the partial-wave amplitudes obtained from the application of fixed-t dispersion relations and crossing symmetry [33]. The pion-nucleon P_{11} amplitude which is responsible for the contribution of pion absorption was treated following the prescription of Ref. [19].

The nucleon-nucleon scattering amplitude t_i taken between partial-wave states (12) is of the same form as that of Eq. (17), except that there is an additional term proportional to $\delta_{l_i,l_i\pm 2}$ that takes into account the coupling between the $^3S_1$ and $^3D_1$ channels. For the nucleon-nucleon partial-wave t matrices $\langle p_i|t_i^{l_i l_i' j_i I_i}(s_i)|p_i'\rangle$ we used separable models that are consistent with the deuteron wave function as given in Ref. [34].

TABLE II. Values of the polarization t_{20}(lab) at $T_\pi = 134$ MeV, $\theta_{\pi,\text{c.m.}}=136°$ determined with absolute and ratio method. The relations for $t_{20}(\theta)$ and $t_{20}(B_{10}), t_{20}(B_{20}), t_{20}(B_{21})$ are stated in the Appendix.

	Absolute		Ratio
$t_{20}(0°)$	-0.592 ± 0.107	$t_{20}(B_{10})$	-0.713 ± 1.044
$t_{20}(25°)$	-0.570 ± 0.158	$t_{20}(B_{20})$	-0.553 ± 0.250
$t_{20}(45°)$	-0.636 ± 0.209	$t_{20}(B_{21})$	-0.489 ± 0.355
total	-0.593 ± 0.081	total	-0.532 ± 0.204

VI. RESULTS

A. Polarizations and analyzing powers

The polarizations were measured with an unpolarized ND_3 target using the experimental setup outlined in Sec. IV. Unpolarized target runs had to be done during the experiment to be independent of the difficult measurement of the ND_3 polarization at thermal equilibrium. Since the polarimeter was designed for the simultaneous use of the absolute and ratio method [28], the polarizations were calculated using both (see Sec. II B and Ref. [28]). The tensor component t_{20} is determined threefold for each method. These values are listed exemplarily in Table II for the incident pion energy $T_\pi = 134$ MeV at $\theta_{\pi,\text{c.m.}}=136°$, showing excellent agreement of the data. The component t_{20} can be determined using the ratio method by three relations [$t_{20}(B_{10}), t_{20}(B_{20})$, and $t_{20}(B_{21})$ which are given in the Appendix], but only two are independent [28]; therefore its error is always larger than by the determination with the absolute method (see Table II). All measured polarization components determined with the absolute method are listed in Table III. The uncertainties quoted include the statistical error resulting from the counting rate statistics as well as systematic errors, coming for example from the polarimeter calibration [28]. Since our results for $iT_{11}(\text{lab}) = iT_{11}(\text{c.m.}) = iT_{11}$ were obtained by a double-scattering experiment the counting rate statistic is small compared to single-scattering experiments and therefore the stated errors are large. Since the transformation of the observables from the laboratory system in the center-of-mass system involves all three tensor polarization components (see Sec. II) the further presented results were determined with the absolute method in order to reduce the error bars.

The analyzing powers were determined by the transformation of the polarizations measured in the laboratory system to the center-of-mass system (see Sec. II). Therefore we have been able to determine $T_{20}(\text{c.m.}) = T_{20}$, $T_{21}(\text{c.m.}) = T_{21}$, $T_{22}(\text{c.m.}) = T_{22}$ and the combined quantities τ_{21} and τ_{22},

TABLE III. Measured polarization components determined with the absolute method. The uncertainties quoted are the statistical as well as the systematic errors.

	$T_\pi = 134$ MeV $\theta_{\pi,\text{c.m.}} = 136°$	$T_\pi = 180$ MeV $\theta_{\pi,\text{c.m.}} = 108°$	$T_\pi = 180$ MeV $\theta_{\pi,\text{c.m.}} = 127°$
$T_{20}(\text{lab}) = t_{20}(\text{lab})$	-0.593 ± 0.081	-0.534 ± 0.049	-0.627 ± 0.083
$T_{21}(\text{lab}) = -t_{21}(\text{lab})$	-0.135 ± 0.154	-0.131 ± 0.109	-0.307 ± 0.206
$T_{22}(\text{lab}) = t_{22}(\text{lab})$	0.146 ± 0.225	-0.415 ± 0.148	0.170 ± 0.236
$T_{20}(\text{c.m.})$	-0.321 ± 0.153	-0.280 ± 0.144	-0.098 ± 0.218
$T_{21}(\text{c.m.})$	-0.403 ± 0.139	-0.154 ± 0.083	-0.559 ± 0.161
$T_{22}(\text{c.m.})$	0.035 ± 0.216	-0.519 ± 0.133	-0.046 ± 0.228
$\tau_{21}(\text{c.m.})$	-0.451 ± 0.179	-0.471 ± 0.110	-0.602 ± 0.202
$\tau_{22}(\text{c.m.})$	-0.096 ± 0.225	-0.633 ± 0.146	-0.086 ± 0.245

$$\tau_{21} = \frac{1}{2}\sqrt{\frac{1}{6}}T_{20} + T_{21} + \frac{1}{2}T_{22},$$

$$\tau_{22} = \sqrt{\frac{1}{6}}T_{20} + T_{22}.$$

Previously the polarizations t_{21}(lab) and t_{22}(lab) and their corresponding analyzing powers T_{21}(c.m.) and T_{22}(c.m.) were only accessible via results from different experiments or using model calculations. Our results of the tensor analyzing powers are listed in Table III. The results for t_{20}(lab) and T_{20} at pion energies of 134 MeV and 180 MeV are shown in Fig. 9 together with data from former experiments. The data from Refs. [5,7,8] are from double-scattering experiments, while the data from Ref. [9] are obtained by a single-scattering experiment. Smith *et al.* used model calculations for the components T_{21} and T_{22}, to obtain t_{20}(lab) $= f(T_{20}, T_{21}, T_{22})$. There is clearly good agreement at the two pion energies between the projected tensor polarizations and analyzing powers of this experiment and previously published data. The predictions of the partial-wave analysis of SAID are based on different databases. The SM94 solution [35] includes elastic πd data while the C500 solution [36] results from a combined analysis of the reactions $pp \leftarrow pp$, $\pi d \leftarrow pp$, and $\pi d \leftarrow pp$. The solid line is the result of phase-shift calculations with SAID using the SM94 solution for the elastic πd channel [35]. In Fig. 10 we present our new data (open circles) for τ_{21} and τ_{22} together with earlier data from single-scattering experiments at TRIUMF and PSI. These experiments used a tensor polarized deuteron target measuring the polarized and unpolarized πd cross section to obtain τ_{21} and τ_{22} while our data were obtained by measuring the tensor polarizations of the recoil deuteron with a double-scattering apparatus. τ_{21} was measured by Smith *et al.* [9] (solid squares), τ_{22} by Ottermann *et al.* [6] (open squares),

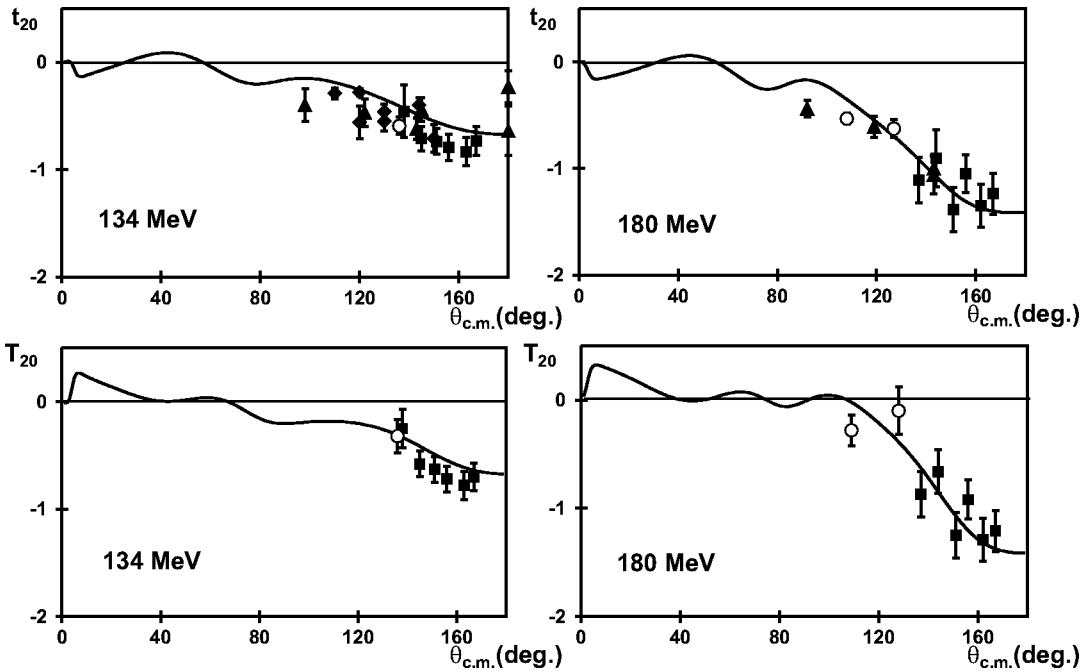

FIG. 9. t_{20} and T_{20} in comparison with previous data. The solid triangles are from Refs. [5,8], the solid diamonds are from Ref. [7], and the solid squares are from Ref. [9]. The data points obtained by this experiment are shown as open circles. The solid line are results from SAID phase-shift analyses (SM94) [35].

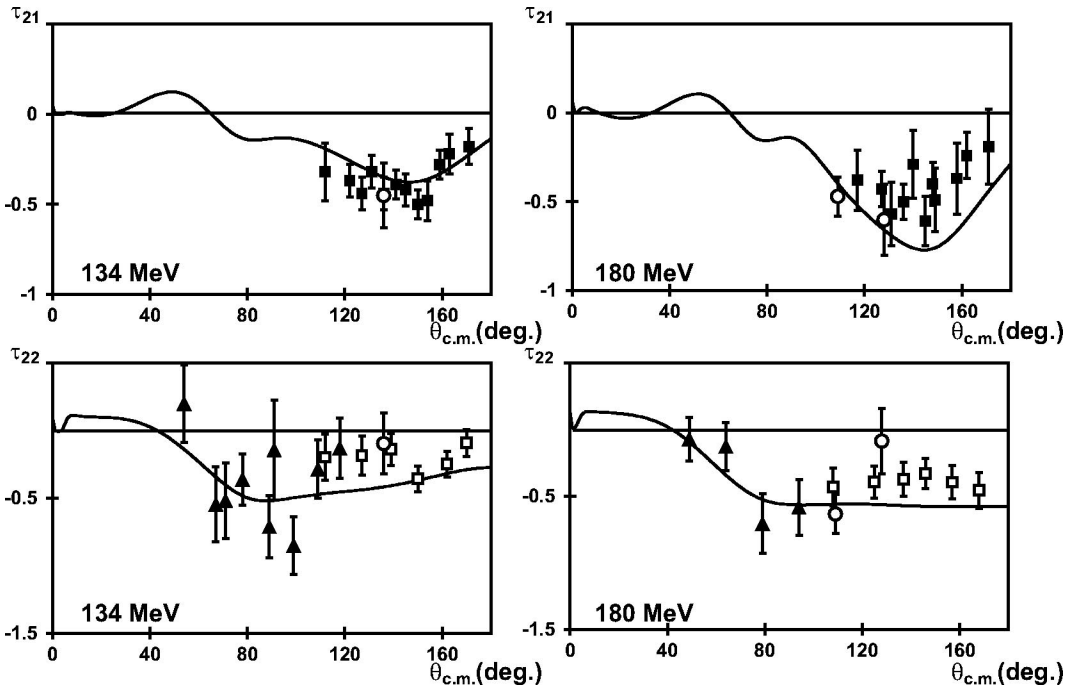

FIG. 10. τ_{21} and τ_{22} (open circles) in comparison with previous data. The solid squares represent previously τ_{21} data of Smith *et al.* [9]. The open squares show results of Ref. [6], the solid triangles of Ref. [3]. The solid line are results from SAID phase-shift analyses (SM94) [35].

and Wessler *et al.* [3] (solid triangles). For our data the quoted uncertainties include both statistical as well as systematic errors, while the data of Wessler *et al.* disregard the systematic error which was stated to be 8% [3]. The solid line represents the SAID SM94 solution [35].

As mentioned before the polarization components t_{21}(lab), t_{22}(lab), respectively, and the analyzing powers T_{21}, T_{22}, were measured up to now only via the combined quantities τ_{21} and τ_{22}. Therefore a direct comparison with former experimental results is not possible. Our measurements are shown in Fig. 11 together with results of the Faddeev calculations (solid line) outlined in Sec. V and results of phase-shift calculations (SAID), with the SM94 solution πd elastic (short dashed line) [35] and the C500 solution of the coupled channels $d(\pi,\pi)d, p(p,p)p$ and $d(\pi,p)p$ (long dashed line) [36]. No major discrepancies exist between the three theoretical results, and also the experimental data are reproduced satisfactorily.

B. Polarization transfer observables

Using a polarized deuteron target with known polarization and measuring the polarization states of the recoil deuteron beam enable us to determine four polarization transfer observables at two different pion energies $T_\pi = 134$ MeV, $\theta_{\text{c.m.}} = 136°$, and $T_\pi = 180$ MeV, $\theta_{\text{c.m.}} = 108°$ and $\theta_{\text{c.m.}} = 127°$. The results are summarized in Table IV. The uncertainties include the statistical errors as well as systematic errors resulting from target and beam polarization measurements. The latter are small compared to the statistical errors. All values are determined using the absolute method following the same reasons outlined above. The precision of the scattering angle is limited by the angular acceptance of the quadrupole triplet and was $\theta(\text{lab}) = \pm 5.5°$. For $\theta_{\pi,\text{c.m.}} = 108°$ at $T_\pi = 180$ MeV the data points were extracted from two different data-taking periods and both datasets are in excellent agreement.

The polarization states of the recoil deuteron beam were measured in the laboratory system and therefore we could obtain the polarization transfer observables in this system. Model calculations and the results of the SAID phase-shift analyses are normally predicted in the center-of-mass frame. As a consequence, the two systems have to be transformed with the equations given in Sec. II; only the observable $(1 \pm 1|11)_{\text{lab}} = (1 \pm 1|11)_{\text{c.m.}}$ is unchanged. Since again all three observables, $i(11|20), i(1 \pm 1|21)$, and $i(1 \pm 1|22)$, are required for the transformation, the errors of the measured quantities are smaller in the laboratory frame. On the other side, the influence of the helicity amplitudes should be more visible in the center-of-mass system. In Fig. 12 the data points are compared to Faddeev calculations and SAID results in the laboratory system, in Fig. 13 in the center-of-mass system. All quantities are according to the Madison convention, which includes an additional sign factor [see Eq. (2)]. This sign factor was not taken into account in our previous publication [37]. Therefore the polarization transfer observables were not stated according to the Madison convention. Additionally the theoretical Faddeev calculations and the SAID predictions were shown in the center-of-mass system while the experimental results were shown in the laboratory system. The solid line in Figs. 12 and 13 represents the results from Faddeev calculations (see Sec. V). The short dashed line gives again the output from the SM94 SAID solution [35] and the long dashed line from the C500 SAID solution [36]. So far, our results are not included in

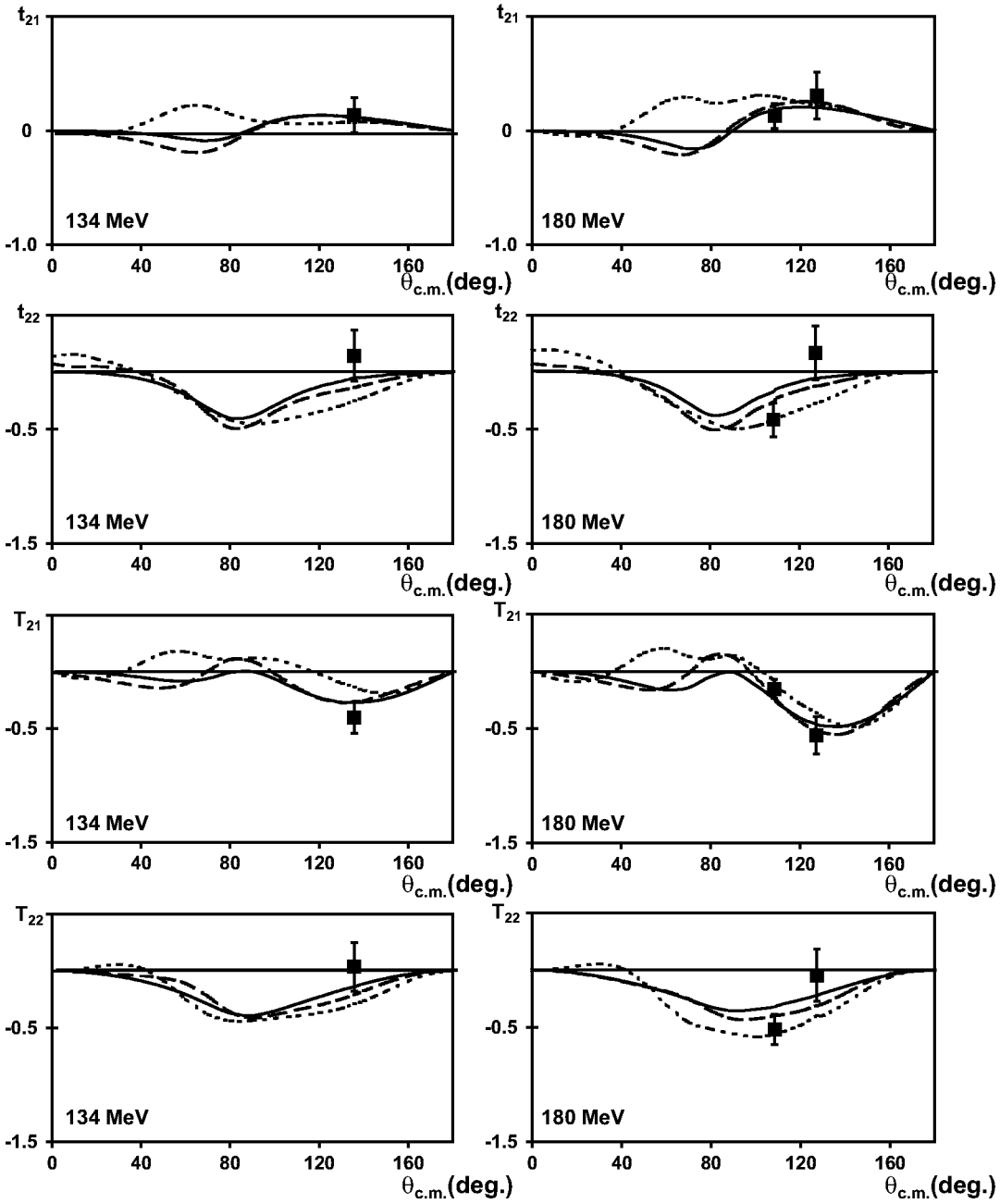

FIG. 11. The tensor polarization components t_{21}(lab),t_{22}(lab) and the tensor analyzing powers T_{21},T_{22} (squares) compared to Faddeev calculations (solid line) and different SAID solutions. The short dashed lines are results from the SM94 solution (elastic πd-channel) [35]; the long dashed lines are from the C500 solution (coupled channels) [36]. All observables are according to the Madison convention.

these databases. The overall good agreement of SM94 and C500 with the measured polarization transfer observables indicates the consistency of these new data with former polarization and analyzing power measurements. The largest deviation between Faddeev calculations and experimental results appears for the observable $i(11|20)$ at 180 MeV in the forward region, while the results of the phase-shift analyses agree quite well.

VII. CONCLUSION

We have measured for the first time a complete set of polarization observables, including polarization transfer, in elastic πd scattering below and at the $\Delta(3,3)$ resonance, at backwards angles. The single scattering observables are in good agreement with the existing world dataset as well as with the SAID predictions SM94 and C500. Polarization transfer has not been measured before.

There are still deviations between the theoretical predictions and experimental data, which also become visible in the helicity amplitudes. A model-independent helicity amplitude analysis has finally become possible, at least for two energies at discrete angles, because the required dataset has now been completed and, even more, overdetermined. Beyond that, this dataset is free of systematic errors resulting

TABLE IV. Measured polarization transfer observables in the laboratory and center-of-mass system.

	$T_\pi = 134$ MeV $\theta_{\pi,\text{c.m.}} = 136°$	$T_\pi = 180$ MeV $\theta_{\pi,\text{c.m.}} = 108°$	$T_\pi = 180$ MeV $\theta_{\pi,\text{c.m.}} = 127°$
$(11\|11)+(1-1\|11)$(lab)	-0.453 ± 0.472	-0.744 ± 0.309	-0.506 ± 0.490
$i(11\|20)$(lab)	0.239 ± 0.119	0.603 ± 0.065	0.135 ± 0.109
$i(11\|21)+i(1-1\|21)$(lab)	-0.005 ± 0.433	0.552 ± 0.271	-0.256 ± 0.488
$i(11\|22)+i(1-1\|22)$(lab)	0.342 ± 0.620	0.373 ± 0.334	0.099 ± 0.585
$(11\|11)+(1-1\|11)$(c.m.)	-0.453 ± 0.472	-0.744 ± 0.309	-0.506 ± 0.490
$i(11\|20)$(c.m.)	0.215 ± 0.216	0.691 ± 0.176	-0.019 ± 0.261
$i(11\|21)+i(1-1\|21)$(c.m.)	-0.089 ± 0.391	-0.355 ± 0.195	-0.246 ± 0.390
$i(11\|22)+i(1-1\|22)$(c.m.)	0.361 ± 0.595	0.301 ± 0.306	0.224 ± 0.562

from different experimental setups or different deuteron target materials.

The polarization transfer observables and additionally the polarizations and analyzing powers determined in this experiment are not included in the SAID databases, neither in SM94 nor in C500. For SM94 we are expecting an improvement of the predictions since the database is relatively small. Therefore the data should have an impact on the predictions of the amplitudes. For the solution C500 the influence should be smaller since the other channels, especially the elastic pp

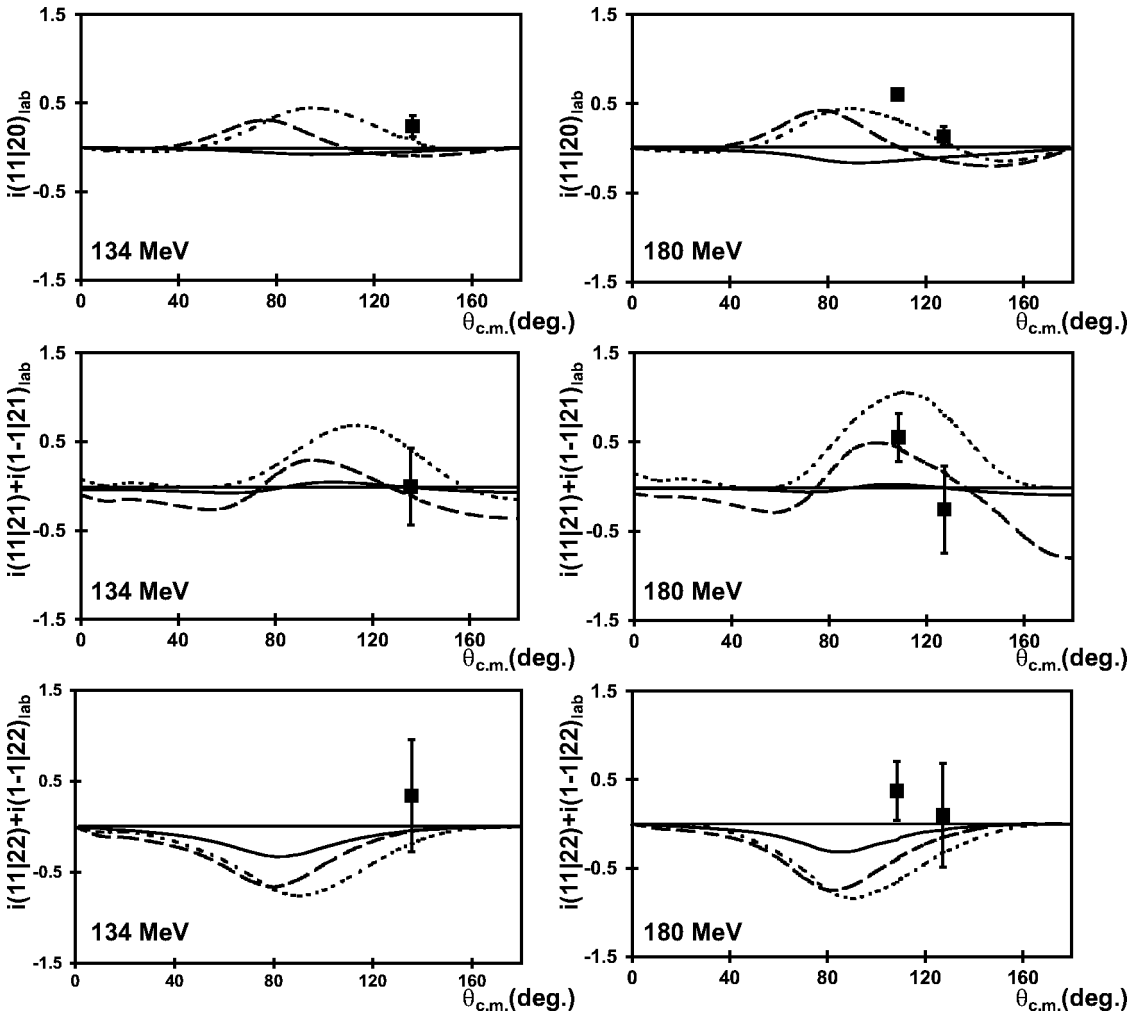

FIG. 12. The polarization transfer observables (squares) in the laboratory system compared to Faddeev calculations (solid line) and different SAID solutions. The short dashed lines are results from the SM94 solution (elastic πd channel) [35]; the long dashed lines are from the C500 solution (coupled channels) [36]. All observables are according to the Madison convention.

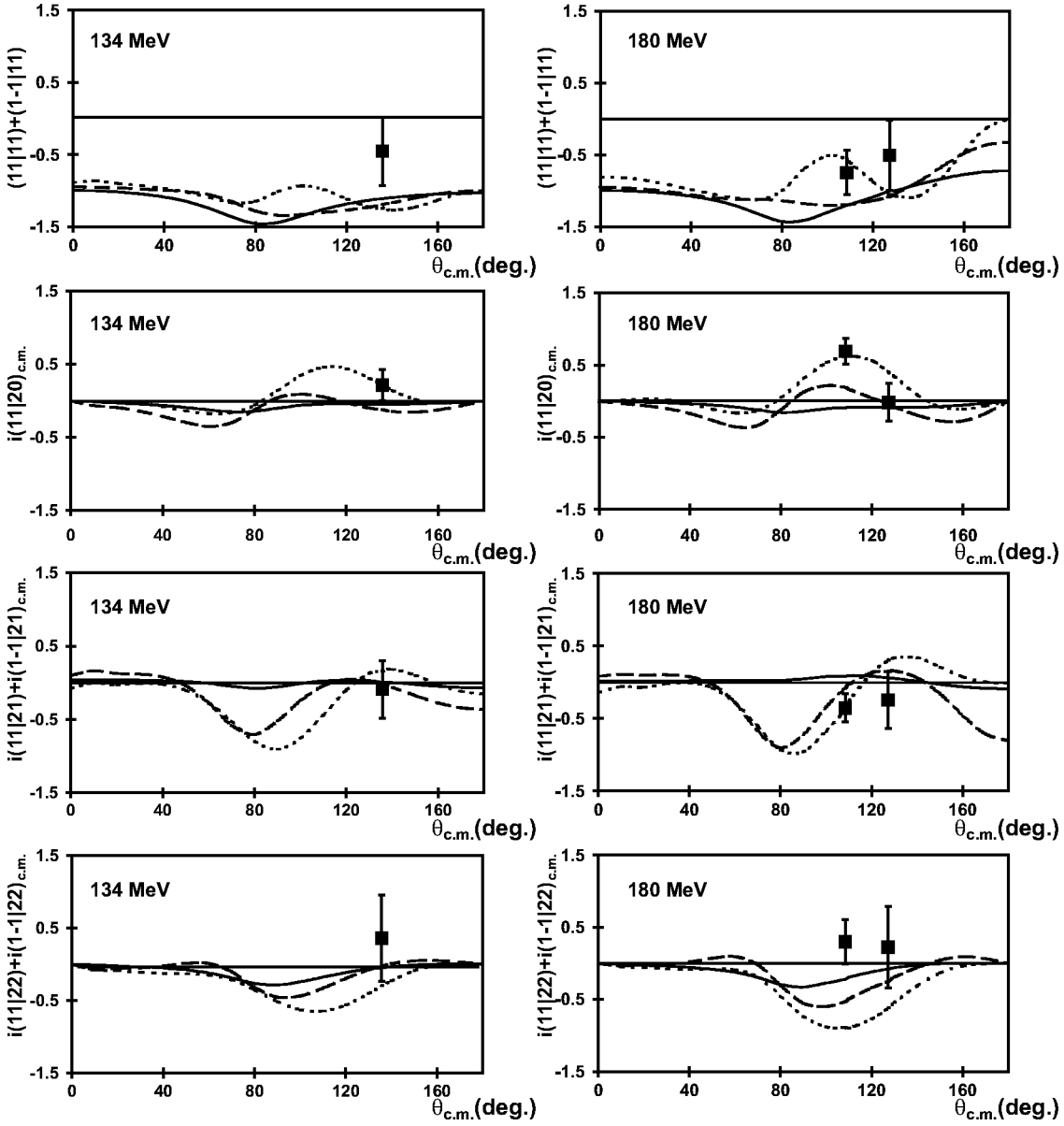

FIG. 13. The polarization transfer observables (squares) in the center-of-mass system compared to Faddeev calculations (solid lines) and different SAID solutions. The short dashed lines are results from the SM94 solution (elastic πd channel) [35]; the long dashed lines are from the C500 solution (coupled channels) [36]. All observables are according to the Madison convention.

channel, have been examined in more detail than the elastic πd channel. Nevertheless, our dataset should enable us to impose some restrictions for the predicted amplitudes.

ACKNOWLEDGMENTS

We would like to express our gratitude to P. Amaudruz, W. Beulertz, A. Bock, M. Frank, A. Glombik, J. Hey, G. Mertens, H. Meyer, L. Sözüer, R. Tacik, and R. Weidmann. Without their help it would have been impossible to carry out this experiment. We would like to thank W. Meyer and his group for irradiating the target material. This work would have been impossible without the generous help and considerable skills of the staff of the PSI. It has been partially funded by the German Federal Ministry for Research and Technology.

APPENDIX

1. Formalism and conventions

The observables for πd elastic scattering are expressed in terms of helicity amplitudes as [24]

$$\frac{d\sigma}{d\Omega} = \tfrac{1}{3}\Sigma \text{ with } \Sigma = 2|A|^2 + 4|B|^2 + 2|C|^2 + |D|^2,$$

$$it_{11} = -i(00|11) = -\sqrt{6}\,\mathrm{Im}[B^*(A - C + D)]/\Sigma,$$

$$t_{20} = (00|20) = \sqrt{2}(|A|^2 + |C|^2 - |B|^2 - |D|^2)/\Sigma,$$

$$t_{21} = -(00|21) = -\sqrt{6}\,\mathrm{Re}[B^*(A - C - D)]/\Sigma,$$

$$t_{22}=(00|22)=\sqrt{3}(2\mathrm{Re}(A^*C)-|B|^2)/\Sigma,$$

$$(11|11)=3(\mathrm{Re}(A^*D)+|B|^2)/\Sigma,$$

$$(11|1-1)=3(-\mathrm{Re}(C^*D)+|B|^2)/\Sigma,$$

$$i(11|20)=-\sqrt{3}\mathrm{Im}[B^*(A-C-2D)]/\Sigma,$$

$$i(11|21)=-3\mathrm{Im}(A^*D)/\Sigma,$$

$$i(11|2-1)=-3\mathrm{Im}(C^*D)/\Sigma,$$

$$i(11|22)=3\sqrt{2}\mathrm{Im}(B^*A)/\Sigma,$$

$$i(11|2-2)=-3\sqrt{2}\mathrm{Im}(B^*C)/\Sigma. \tag{A1}$$

Application of Eq. (1) to the observables of Eq. (A1) leads to the following expressions:

$$iT_{11}^{\mathrm{lab}}=-it_{11}^{\mathrm{lab}}=iT_{11}^{\mathrm{c.m.}},$$

$$T_{20}^{\mathrm{lab}}=t_{20}^{\mathrm{lab}}=\frac{3\cos^2\theta_R-1}{2}T_{20}^{\mathrm{c.m.}}+2\sqrt{\frac{3}{2}}\sin\theta_R\cos\theta_R T_{21}^{\mathrm{c.m.}}+\sqrt{\frac{3}{2}}\sin^2\theta_R T_{22}^{\mathrm{c.m.}},$$

$$T_{21}^{\mathrm{lab}}=-t_{21}^{\mathrm{lab}}=-\sqrt{\frac{3}{2}}\sin\theta_R\cos\theta_R T_{20}^{\mathrm{c.m.}}+(2\cos^2\theta_R-1)T_{21}^{\mathrm{c.m.}}+\sin\theta_R\cos\theta_R T_{22}^{\mathrm{c.m.}},$$

$$T_{22}^{\mathrm{lab}}=t_{22}^{\mathrm{lab}}=\frac{1}{2}\sqrt{\frac{3}{2}}\sin^2\theta_R T_{20}^{\mathrm{c.m.}}-\sin\theta_R\cos\theta_R T_{21}^{\mathrm{c.m.}}+\frac{1+\cos^2\theta_R}{2}T_{22}^{\mathrm{c.m.}},$$

$$i(1\pm1|11)_{\mathrm{lab}}=i(1\pm1|11)_{\mathrm{c.m.}},$$

$$i(11|20)_{\mathrm{lab}}=\frac{3\cos^2\theta_R-1}{2}i(11|20)_{\mathrm{c.m.}}-\sqrt{\frac{3}{2}}\sin\theta_R\cos\theta_R i(1\pm1|21)_{\mathrm{c.m.}}+\frac{1}{2}\sqrt{\frac{3}{2}}\sin^2\theta_R i(1\pm1|22)_{\mathrm{c.m.}},$$

$$i(1\pm1|21)_{\mathrm{lab}}=\sqrt{6}\sin\theta_R\cos\theta_R i(11|20)_{\mathrm{c.m.}}+(2\cos^2\theta_R-1)i(1\pm1|21)_{\mathrm{c.m.}}-\sin\theta_R\cos\theta_R i(1\pm1|22)_{\mathrm{c.m.}},$$

$$i(1\pm1|22)_{\mathrm{lab}}=\sqrt{\frac{3}{2}}\sin^2\theta_R i(11|20)_{\mathrm{c.m.}}+\sin\theta_R\cos\theta_R i(1\pm1|21)_{\mathrm{c.m.}}+\frac{1+\cos^2\theta_R}{2}i(1\pm1|22)_{\mathrm{c.m.}}, \tag{A2}$$

where

$$i(1\pm1|L'M')=i(11|L'M')+i(1-1|L'M').$$

The polarization transfer observables choosing a Cartesian coordinate system are

$$K_y^{y'}=\frac{1}{3p_Z}\left[\frac{p^+_{y'}\sigma^+-p^-_{y'}\sigma^-}{\sigma^0}\right],$$

$$K_y^{x'z'}=\frac{1}{3p_Z}\left[\frac{p^+_{x'z'}\sigma^+-p^-_{x'z'}\sigma^-}{\sigma^0}\right],$$

$$K_y^{x'x'}=\frac{1}{3p_Z}\left[\frac{p^+_{x'x'}\sigma^+-p^-_{x'x'}\sigma^-}{\sigma^0}\right],$$

$$K_y^{y'y'}=\frac{1}{3p_Z}\left[\frac{p^+_{y'y'}\sigma^+-p^-_{y'y'}\sigma^-}{\sigma^0}\right],$$

$$K_y^{z'z'}=\frac{1}{3p_Z}\left[\frac{p^+_{z'z'}\sigma^+-p^-_{z'z'}\sigma^-}{\sigma^0}\right],$$

with

$$K_y^{x'x'}+K_y^{y'y'}+K_y^{z'z'}=0.$$

They are related to the spherical observables by

$$(11|11)^{\mathrm{Mad}}+(1-1|11)^{\mathrm{Mad}}=-\frac{3}{2}K_y^{y'},$$

$$i(11|20)^{\mathrm{Mad}}=-\sqrt{\frac{3}{2\sqrt{2}}}K_y^{z'z'},$$

$$i(11|21)^{\mathrm{Mad}}+i(1-1|21)^{\mathrm{Mad}}=-K_y^{x'z'},$$

$$i(11|22)^{\mathrm{Mad}}+i(1-1|22)^{\mathrm{Mad}}=-\frac{1}{2}(K_y^{x'x'}-K_y^{y'y'}).$$

2. The polarization of the deuterons

The deuteron polarimeter measures the number of protons emitted in the scattering angles $\theta=0°,25°,45°$ and in the azimuthal angles $\phi=0°,90°,180°,270°$. The corresponding counting rates are labeled $L(\theta_i),D(\theta_i),R(\theta_i),U(\theta_i)$ ($\theta_i\in\{25°,45°\}$) and $N(0°)$ for the 0° detector. The counting rates in the polarimeter detectors can be calculated using Eq. (5):

$$L(\theta_i)=\sigma_0[1+2it_{11}iT_{11}(\theta_i)+t_{20}T_{20}(\theta_i)+2t_{21}T_{21}(\theta_i)+2t_{22}T_{22}(\theta_i)],$$

$$R(\theta_i)=\sigma_0[1-2it_{11}iT_{11}(\theta_i)+t_{20}T_{20}(\theta_i)-2t_{21}T_{21}(\theta_i)+2t_{22}T_{22}(\theta_i)],$$

$$D(\theta_i)=\sigma_0[1+t_{20}T_{20}(\theta_i)-2t_{22}T_{22}(\theta_i)],$$

$$U(\theta_i)=\sigma_0[1+t_{20}T_{20}(\theta_i)-2t_{22}T_{22}(\theta_i)],$$

$$N(0°)=\sigma_0[1+t_{20}T_{20}(0°)]. \quad \text{(A3)}$$

a. The absolute method

The following asymmetries and count rates have to be defined to determine the deuteron polarization ($\theta_i \in \{25°,45°\}$):

$$A_1(\theta_i)=L(\theta_i)-R(\theta_i)=4\sigma_0[it_{11}iT_{11}(\theta_i)+t_{21}T_{21}(\theta_i)],$$

$$A_2(\theta_i)=[L(\theta_i)+R(\theta_i)]-[U(\theta_i)+D(\theta_i)]=8\sigma_0 t_{22}T_{22}(\theta_i),$$

$$N(\theta_i)=L(\theta_i)+R(\theta_i)+U(\theta_i)+D(\theta_i)=4\sigma_0[1+t_{20}T_{20}(\theta_i)],$$

$$N(0°)=\sigma_0[1+t_{20}T_{20}(0°)].$$

Additionally, the number of deuterons N_d incident on the ^{3}He cell is required. The polarimeter efficiencies $r(\theta)$ are defined by

$$r^0(\theta)=\frac{N^0(\theta)}{N_d^0}, \quad r(\theta)=\frac{N(\theta)}{N_d}, \quad \theta\in\{0°,25°,45°\};$$

$r^0(\theta)$ are the polarimeter efficiencies with unpolarized deuteron beam, resulting from an independent polarimeter calibration. The tensor component t_{20} can be determined threefold:

$$t_{20}(\theta)=\frac{1}{T_{20}(\theta)}\left(\frac{r(\theta)}{r^0(\theta)}-1\right), \quad \theta\in\{0°,25°,45°\};$$

t_{22} is calculated independently from the counting rates in the detectors at $\theta_i=25°$ and $\theta_i=45°$:

$$t_{22}(\theta_i)=\frac{1}{T_{22}(\theta_i)}\frac{A_2(\theta_i)}{2r^0(\theta_i)N_d}$$

it_{11} and t_{21} are resulting from the left-right asymmetry:

$$it_{11}=\frac{1}{N_d}\frac{\frac{A_1(25°)T_{21}(45°)}{r^0(25°)}-\frac{A_1(45°)T_{21}(25°)}{r^0(45°)}}{iT_{11}(25°)T_{21}(45°)-iT_{11}(45°)T_{21}(25°)},$$

$$t_{21}=-\frac{1}{N_d}\frac{\frac{A_1(25°)iT_{11}(45°)}{r^0(25°)}-\frac{A_1(45°)iT_{11}(25°)}{r^0(45°)}}{iT_{11}(25°)T_{21}(45°)-iT_{11}(45°)T_{21}(25°)}.$$

b. The ratio method

In analogy to the absolute method asymmetries are defined, but only the ratio of the counting rates at different scattering and azimuthal angles are regarded. Therefore the number of incoming deuterons is not required.

$$B_{10}=\frac{N(25°)}{N(0°)}=4\frac{I_0(25°)[1+t_{20}T_{20}(25°)]}{I_0(0°)[1-t_{20}T_{20}(0°)]},$$

$$B_{20}=\frac{N(45°)}{N(0°)}=4\frac{I_0(45°)[1+t_{20}T_{20}(45°)]}{I_0(0°)[1-t_{20}T_{20}(0°)]},$$

$$B_{21}=\frac{N(45°)}{N(25°)}=\frac{I_0(45°)[1+t_{20}T_{20}(45°)]}{I_0(25°)[1-t_{20}T_{20}(25°)]},$$

$$B_1(\theta_i)=\frac{L(\theta_i)-R(\theta_i)}{N(\theta_i)}=\frac{it_{11}iT_{11}(\theta_i)+t_{21}T_{21}(\theta_i)}{1+t_{20}T_{20}(\theta_i)},$$

$$B_2(\theta_i)=\frac{[L(\theta_i)+R(\theta_i)]-[U(\theta_i)+D(\theta_i)]}{N(\theta_i)}=2\frac{t_{22}T_{22}(\theta_i)}{1+t_{20}T_{20}(\theta_i)}.$$

The ratios B_{10}, B_{20}, and B_{21} are linearly dependent, because $B_{20}=B_{10}B_{21}$. Three values of t_{20} can be determined, but only two of them are linearly independent:

$$t_{20}(B_{10})=\frac{(B_{10}/B_{10}^0)-1}{T_{20}(25°)-(B_{10}/B_{10}^0)T_{20}(0°)},$$

$$t_{20}(B_{20})=\frac{(B_{20}/B_{20}^0)-1}{T_{20}(45°)-(B_{20}/B_{20}^0)T_{20}(0°)},$$

$$t_{20}(B_{21})=\frac{(B_{21}/B_{21}^0)-1}{T_{20}(45°)-(B_{21}/B_{21}^0)T_{20}(25°)}.$$

The subscript zero denotes ratios coming from the polarimeter calibration, with

$$B_{10}^0=\frac{r^0(25°)}{r^0(0°)}, \quad B_{20}^0=\frac{r^0(45°)}{r^0(0°)}, \quad B_{21}^0=\frac{r^0(45°)}{r^0(25°)};$$

The two values of t_{22} are calculated from independent counting rates at different scattering angles ($\theta_i=25°,45°$) in the polarimeter. it_{11} and t_{21} result from the left-right asymmetry:

$$t_{22}(\theta_i)=\frac{B_2(\theta_i)}{2T_{22}(\theta_i)}[1+t_{20}T_{20}(\theta_i)],$$

$$it_{11}=\frac{B_1(25°)T_{21}(45°)[1+t_{20}T_{20}(25°)]}{iT_{11}(25°)T_{21}(45°)-iT_{11}(45°)T_{21}(25°)}$$
$$-\frac{B_1(45°)T_{21}(25°)[1+t_{20}T_{20}(45°)]}{iT_{11}(25°)T_{21}(45°)-iT_{11}(45°)T_{21}(25°)},$$

$$t_{21}=-\frac{B_1(25°)iT_{11}(45°)[1+t_{20}T_{20}(25°)]}{iT_{11}(25°)T_{21}(45°)-iT_{11}(45°)T_{21}(25°)}$$
$$+\frac{B_1(45°)iT_{11}(25°)[1+t_{20}T_{20}(45°)]}{iT_{11}(25°)T_{21}(45°)-iT_{11}(45°)T_{21}(25°)}.$$

[1] H. Garcilazo, T. Mizutani, *πNN Systems* (World Scientific, Singapore, 1990).

[2] K. Gabathuler, J. Domingo, P. Gram, W. Hirt, G. Jones, P. Schwaller, J. Zichy, J. Bolger, Q. Ingram, J.P. Albanese, and J. Arvieux, Nucl. Phys. **A350**, 253 (1980); C.R. Ottermann, E.T. Boschitz, W. Gyles, W. List, R. Tacik, R.R. Johnson, G.R. Smith, and E.L. Mathie, Phys. Rev. C **32**, 928 (1985).

[3] M. Wessler, E. Boschitz, B. Brinkmöller, J. Bühler, H. Garcilazo, W. Gyles, W. List, R. Meier, S. Ritt, T. Tacik, J.A. Konter, D. Gill, S. Mango, D. Renker, B. van den Brandt, G. Wait, V.A. Efimovykh, A.I. Kovalev, A.N. Prokofiev, W. Thiel, and B. Blankleider, Phys. Rev. C **51**, 2575 (1995).

[4] G.R. Smith, E.L. Mathie, E.T. Boschitz, C.R. Ottermann, S. Mango, J.A. Konter, M. Daum, M. Meyer, R. Olszewski, and F. Vogler, Phys. Rev. C **29**, 2206 (1984).

[5] R.J. Holt, J.R. Specht, E.J. Stephenson, B. Zeidman, R.L. Burman, J.S. Frank, M.J. Leitch, J.D. Moses, M.A. Yates-Williams, R.M. Laszewski, and R.P. Redwine, Phys. Rev. Lett. **43**, 1229 (1979); R.J. Holt, J.R. Specht, K. Stephenson, B. Zeidman, J.S. Frank, M.J. Leitch, J.D. Moses, E.J. Stephenson, and R.M. Laszewski, *ibid.* **47**, 472 (1981).

[6] C.R. Ottermann, E.T. Boschitz, H. Garcilazo, W. Gyles, W. List, R. Tacik, M. Wessler, S. Mango, B. van den Brandt, J.A. Konter, and E.L. Mathie, Phys. Rev. C **38**, 2310 (1988).

[7] N.R. Stevenson, Y.M. Shon, K. Itoh, G. Retzlaff, D.R. Gill, D.F. Ottewell, G.D. Wait, T.E. Drake, D. Frekers, R.B. Schubank, and G.J. Lolos, Phys. Rev. C **39**, 1488 (1989).

[8] E. Ungricht, W.S. Freeman, D.F. Geesaman, R.J. Holt, J.R. Specht, B. Zeidman, E.J. Stephenson, J.D. Moses, M. Farkhondeh, S. Gilad, and R.P. Redwine, Phys. Rev. C **31**, 934 (1985).

[9] G.R. Smith, D.R. Gill, D. Healey, D. Ottewell, G.D. Wait, P. Walden, R.R. Johnson, G. Jones, R. Olszewski, F.M. Rozon, R. Rui, M.E. Sevior, R.P. Trelle, E.L. Mathie, G.J. Lolos, C.R. Ottermann, W. Gyles, and G.S. Kyle, Phys. Rev. C **35**, 2343 (1987); G.R. Smith, D.R. Gill, D. Healey, D. Ottewell, G.D. Wait, P. Walden, R.R. Johnson, G. Jones, R. Olszewski, F.M. Rozon, R. Rui, M.E. Sevior, R.P. Trelle, E.L. Mathie, G.J. Lolos, S.I.H. Naqvi, V. Pafilis, N.R. Stevenson, R.B. Schubank, W. Gyles, C.R. Ottermann, and G.S. Kyle, *ibid.* **38**, 251 (1988).

[10] Y.M. Shin, K. Itoh, N.R. Stevenson, D.R. Gill, D.F. Ottewell, G.D. Wait, T.E. Drake, D.F. Frekers, R.B. Schubank, and G.J. Lolos, Phys. Rev. Lett. **55**, 2672 (1985).

[11] Y. Avishai, T. Mizutani, Nucl. Phys. **A326**, 352 (1979).

[12] B. Blankleider and I.R. Afnan, Phys. Rev. C **24**, 1572 (1981).

[13] A.S. Rinat, Y. Starkand, and E. Hammel, Nucl. Phys. **A364**, 486 (1981).

[14] H. Garcilazo, Nucl. Phys. **A360**, 411 (1981).

[15] S.C.B. Andrade, E. Ferreira, and H.G. Dosch, Phys. Rev. C **34**, 226 (1986); E. Ferreira, S.C.B. de Andrade, and H.G. Dosch, *ibid.* **36**, 1916 (1987); E. Ferreira and H.G. Dosch, *ibid.* **40**, 1750 (1989).

[16] K. Kanai, A. Minaka, A. Nakamura, and H. Sumiyoshi, Prog. Theor. Phys. **62**, 153 (1979).

[17] C. Alexandrou and B. Blankleider, Phys. Rev. C **42**, 517 (1990).

[18] H. Garcilazo, E.T. Boschitz, W. Gyles, W. List, C.R. Ottermann, R. Tacik, and M. Wessler, Phys. Rev. C **39**, 942 (1989).

[19] H. Garcilazo, Phys. Rev. C **35**, 1804 (1987).

[20] B.K. Jennings, Phys. Lett. B **205**, 187 (1988); B.K. Jennings and A.S. Rinat, Nucl. Phys. **A485**, 421 (1988).

[21] T. Mizutani, C. Fayard, G.H. Lamot, and B. Saghai, Phys. Rev. C **40**, 2763 (1989).

[22] A.N. Kvinikhidze and B. Blankleider, Nucl. Phys. **A574**, 788 (1994).

[23] M. Jacob and G.C. Wick, Ann. Phys. (N.Y.) **7**, 404 (1959).

[24] W. Grein and M.P. Locher, J. Phys. G **7**, 1355 (1981).

[25] F. Pereira and E. Ferreira, J. Phys. G **12**, 1389 (1986).

[26] M.E. Rose, *Elementary Theory of Angular Momentum* (Wiley, New York, 1957).

[27] G.G. Ohlsen, Rep. Prog. Phys. **35**, 717 (1972).

[28] W. Grüebler, V. König, P.A. Schmelzbach, M. Bittcher, B. Vuaridel, Ch. Forstner, D. Singy, I. Slaus, and A. Chrisholm, Nucl. Instrum. Methods Phys. Res. A **262**, 307 (1987).

[29] H. Garcilazo and L. Mathelitsch, Nucl. Phys. **A591**, 639 (1995).

[30] H. Garcilazo, J. Math. Phys. **27**, 2576 (1986).

[31] M. Lacombe, B. Loiseau, R. Vinh Mau, J. Cote, P. Pires, and R. de Tourreil, Phys. Lett. **101B**, 139 (1981).

[32] R.A. Arndt, R.L. Workman, Z. Li, and L.D. Roper, Phys. Rev. C **42**, 1853 (1990).

[33] H. Nielsen and G.C. Oades, Nucl. Phys. **B49**, 573 (1972).

[34] H. Garcilazo, Phys. Rev. C **47**, 957 (1993).

[35] R.A. Arndt, I.I. Strakovsky, and R.L. Workman, Phys. Rev. C **50**, 1796 (1994).

[36] C.-H. Oh, R.A. Arndt, I.I. Strakovsky, and R.L. Workman, Phys. Rev. C **56**, 635 (1997).

[37] G. Suft, P. Amaudruz, E. Boschitz, B. van den Brandt, B. Brinkmöller, A. Glombik, J. Goetz, W. Grüebler, P. Hautle, J.A. Konter, W. Kretschmer, M. Lauterbach, S. Mango, R. Meier, C. Riedel, R. Tacik, and R. Weidmann, Phys. Lett. B **425**, 19 (1998).